Kovove Mater. 61 2023 369–383
DOI: 10.31577/km.2023.6.369

Study of high-temperature deformation behavior and thermal processing diagram of cast TA15 titanium alloy

Yanchun Zhu[1], Zhiquan Huang[1]*, Jiaxin Fan[1]**, Ling Qin[2], Yong Niu[1]

[1] *School of Mechanical Engineering, Taiyuan University of Science and Technology, Taiyuan 030024, P. R. China*
[2] *Center of Innovation for Flow Through Porous Media, Department of Petroleum Engineering, University of Wyoming, Laramie, WY, 82071, USA*

Received 2 June 2022, received in revised form 30 May 2023, accepted 16 June 2023

Abstract

In this study, the high-temperature deformation behavior of cast TA15 titanium alloy was investigated by thermal simulation compression experiments. The heat deformation temperatures ranged from 1323 to 1473 K, and the strain rates were 0.1, 1.0, and 10 s^{-1}. The results show that the softening mechanism of cast TA15 titanium alloy is mainly local plastic flow when deformed at a high strain rate ($\dot{\varepsilon} = 10\,s^{-1}$); at a low strain rate ($\dot{\varepsilon} \leq 1.0\,s^{-1}$), it is mainly dynamic reversion and dynamic recrystallization. The developed constitutive equation that takes into account the effects of strain can accurately describe the rheological behavior of TA15 alloy over the entire stress range. The correlation coefficient r of 0.95637 and the average relative error ARE of 6.45 % were calculated between the flow stress values of the alloy during thermal deformation and the calculated values of the model, indicating that the model constructed in this study is more accurate. The optimal high-temperature deformation processing window was obtained using the thermal processing diagram and combined with the microstructure of the deformed specimens: deformation temperature 1373–1423 K and strain rate 0.1–1.0 s^{-1}.

K e y w o r d s: cast TA15 titanium alloy, high-temperature deformation behavior, constitutive model, thermal processing diagram

1. Introduction

TA15 titanium alloy is developed on the basis of Russian BT20 alloy [1], which belongs to a high--alumina near-alpha titanium alloy with β-stable elements such as Mo and V. It has the advantages of high strength-to-weight ratio, excellent creep and erosion resistance, excellent high-temperature mechanical properties and welding properties, and has been widely used in the aerospace industry as a key weighing component of aircraft [2], for example, high-stress parts of aero-engines, frames, compressor blades, and turbine blades, Xu et al. [3]. At present, experts, scholars, and research institutions in various countries have conducted a lot of research on the high--temperature deformation mechanism, microstructure evolution, mechanical properties of TA15 titanium alloy, and other factors affecting the application of the material. Li et al. [4] investigated the collective behavior and mechanism of slip activity, slip transfer, and grain boundary slip in the tri-modal microstructure of TA15 titanium alloy by quasi-in-situ tensile testing, SEM, EBSD, and quantitative slip trace analysis. The microscopic deformation mechanism of TA15 titanium alloy with a trimodal organization is revealed to be important for improving its mechanical properties. Similarly, Gao et al. [5] also investigated the mechanical properties of TA15 titanium alloy with a trimodal organization in relation to the tissue parameters. A black propagation neural network model is developed to correlate the mechanical properties with the microstructural parameters of the trimodal microstructure. A better combination of strength and plasticity can be achieved. Ma et al. [6] investigated the static softening behavior and dislocation density evolution of TA15 titanium alloy during double pass subther-

*Corresponding author: e-mail address: 2014247@tyust.edu.cn
**Corresponding author: e-mail address: fanjiaxin686@163.com

Table 1. Chemical composition of TA15 titanium alloy

Element	Al	V	Mo	Zr	Fe	Ti
Content	6.6	2.3	1.7	2.2	0.06	Balance

mal deformation, and by observing the microstructure after deformation, it was found that the incipient α-phase showed spheroidal behavior and various crystalline surfaces of the α-phase, and the dislocation density between the layers gradually decreased with the increase of holding time and deformation temperature. Wang et al. [7] investigated the effect of recrystallization on the thermal deformation mechanism of TA15 titanium alloy using the uniaxial tensile test and biaxial gas expansion test, respectively. Yasmeen et al. [8] achieved the maximum mesh aspect ratio by simulating the superplasticity mechanism of TA15 alloy with equiaxed, fine grain structure and applying the proposed intrinsic model to study TA15 sheets with an initial thickness of 1.2 mm in superplastic forming (SPF). Arab et al. [9] obtained the microstructure of four different TA15 titanium alloys using different heat treatment conditions and then studied the hardness and dynamic behavior of these specimens to investigate the relationship between microstructure and mechanical properties. The results showed that the water-quenched specimens with martensitic α structure had the highest hardness, and the bimodal organization showed good plastic deformation and proper strength. Zhu et al. [10] revealed the effect of deformation conditions on the two parameters by studying the strain rate sensitivity exponent and strain hardening exponent of high-temperature deformation of cast TA15 titanium alloy.

However, the low plasticity of TA15 titanium alloy and the high flow stress under high-temperature conditions make it difficult to deform and machine, and the reasonable processing window is relatively narrow. Therefore, in this study, the high-temperature deformation behavior of cast TA15 titanium alloy was studied based on thermal simulation and compression experiments; the intrinsic constitutive equations of high-temperature deformation of cast TA15 titanium alloy under different strains were constructed, and error analysis was carried out; by establishing the thermal processing diagram of the alloy and combining the microstructure of the specimens after deformation under different deformation conditions, a reasonable processing window for high-temperature deformation of cast TA15 titanium alloy was finally optimized, which can provide some guidance for practical production.

2. Experiments and methods

The material used in this study is the cast TA15 titanium alloy, whose chemical composition is shown in Table 1. Its main strengthening mechanism is through solid solution strengthening of α-stable elements Al, adding neutral elements Zr and β-stable elements Mo and V to improve the process properties. Based on the binary phase diagram calculation method and differential scanning calorimetry (DSC), the phase transition point of the as-cast TA15 titanium alloy is about 1268 K. The original microstructure is shown in Fig. 1.

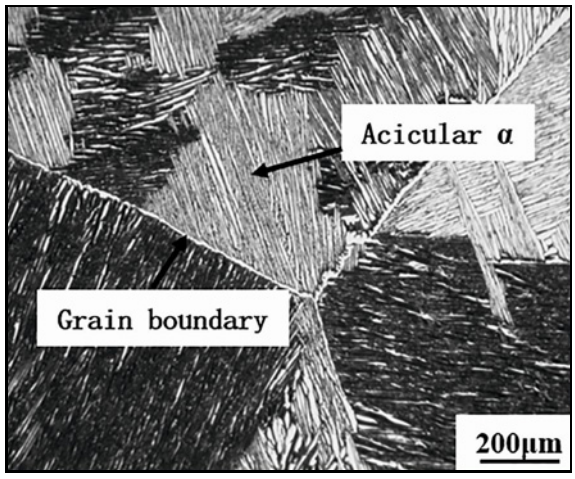

Fig. 1. Original cast organization of cast TA15 titanium alloy.

In the thermal simulation compression test conducted in this study, a Gleeble-1500D thermal simulation compression tester was used to perform compression tests on the cast TA15 titanium alloy with a cylinder size of ø 10 mm × 15 mm. In this experiment, in order to prevent the "bulging" of the specimen caused by uneven deformation, tantalum pads were placed on both ends of the specimen during compression to reduce the friction between the indenter and the specimen. The specimens were heated to the deformation temperature at a heating rate of 10 ℃ s^{-1}, held for 5 min, and then isothermally deformed to ensure the uniform temperature of the specimens and eliminate the internal stress [11]. The specific deformation conditions and the experimental flow chart are shown in Fig. 2. The true stress-true strain data under different deformation conditions were obtained by a special data acquisition system configured with the Gleeble-1500D hot compression simulation tester, and the flow stress-strain curves of cast TA15 titanium alloy under different deformation conditions were plotted by *Origin software*.

The preparation of titanium alloy specimens without distorted surfaces is the basis for the microstructure characterization of all titanium alloys [12]. Firstly, the isothermal compressed (cooled) specimens were cut along the axial direction with DK7735 tapered wire cutter (as shown in Fig. 3) and were se-

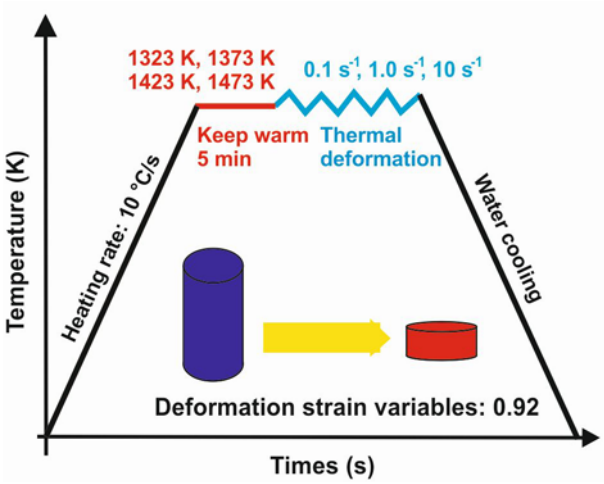

Fig. 2. Thermal compression simulation experimental conditions and experimental flow chart.

Fig. 3. Wire-cutting machine.

T a b l e 2. Kroll corrosion fluid composition and ratio used in this test

Ingredients	HF	HNO_3	H_2O
Volume fractions	2 %	6 %	Balance

quentially subjected to coarse grinding, fine grinding, electrolytic polishing, etching, and finally, microstructure observation. It should be noted that during the grinding process from coarse to fine grinding, the sandpaper can be properly wetted, the main purpose of which is to prevent the titanium alloy from having twin formation on the surface of the titanium alloy due to the violent friction that makes the temperature rise and affects the tissue observation [12]. The finely ground titanium alloy specimens were electrolytically polished in an electrolyte with a volume fraction of 34 % n-butanol, 6 % perchloric acid, and 60 % methanol at a voltage of 45 V and a current density of 1 A mm^{-2}. The electrolyte was cooled down to below –10 ℃ for 25 s using liquid nitrogen, and a magnetic mixer was used to ensure the flow of the electrolyte. Finally, the electrolytically polished cast TA15 titanium alloy specimens were corroded using Kroll reagent (see Table 2 for the main components and ratios) with an erosion time of 10 s. It is worth noting that the original state tissue of cast TA15 titanium alloy can be simply wiped with a cotton swab on the surface of the titanium alloy and should not be eroded in the corrosion solution for a long time.

The final treated specimens were observed under an optical microscope, mainly to observe the morphology of the alloy, the change of grain boundaries, and the appearance of dynamically recrystallized grains at the grain boundaries.

3. Results and discussion

3.1. Flow stress behavior

The true stress-true strain curves of TA15 titanium alloy obtained from hot compression tests at different temperatures and strain rates are shown in Fig. 4. As can be seen from Fig. 4, the rheological stress of TA15 titanium alloy has a similar trend at different strain rates and different temperatures. The rheological stresses all rise rapidly to a peak at the beginning of deformation, go through a period of stability, and then fall rapidly. At the same strain rate and strain conditions, the flow stress shows a decreasing trend with increasing temperature, which indicates that the temperature has a significant effect on the softening of TA15 alloy and is also favorable for dynamic recovery and recrystallization. This typical phenomenon has been found in the study of the rheological behavior of other titanium alloys [11, 13–15]. At the same temperature, the lower the strain rate, the lower the rheological stress. This is because at the same temperature, as the strain rate decreases, the deformation time increases, allowing the deformation and the thermal softening process to proceed fully, resulting in a significant reduction in stress at low strain rates compared to high strain rates, and demonstrating the strong sensitivity of TA15 alloy to strain rate. At the early stage of deformation, the alloy rheological stress increases rapidly with the increase of the strain, and this phenomenon is mainly attributed to the result of competition between work hardening and dynamic softening [14], as the internal dislocations of the alloy increase with the increase of the strain at this deformation stage, the work hardening effect is enhanced and

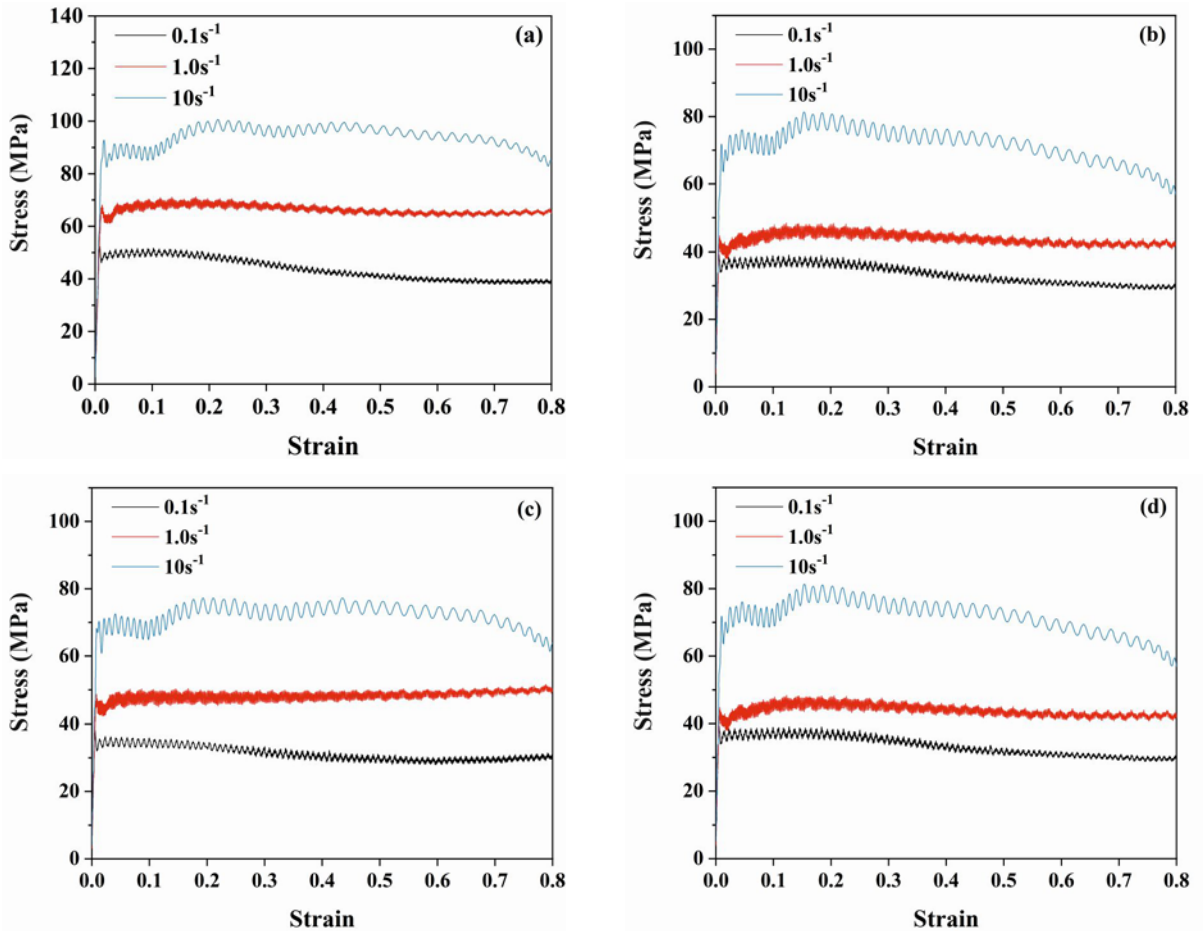

Fig. 4. Flow stress-strain curves of cast TA15 titanium alloy under different deformation conditions: (a) 1323 K, (b) 1373 K, (c) 1423 K, and (d) 1473 K.

exceeds the dynamic softening, resulting in a rapid increase of the stress; as the deformation proceeds, the thermal softening effect is enhanced, making the two reach a dynamic equilibrium and the flow stress gradually tends to a stable state. At the same strain rate, the higher the temperature, the lower the rheological stress and the lower the peak stress. Since the deformation process occurs in the β single-phase region and β is a body-centered cubic structure with more slip systems and high layer misalignment energy, the intergranular shear resistance decreases as the deformation temperature increases, leading to easier deformation and lower rheological stresses.

From the above figure, it can be seen that almost all flow stress-strain curves show different degrees of softening effect; the higher the strain rate and the higher the temperature, the greater the decreased value of the curve, both and the softening effect of the material is more obvious. Due to the poor thermal conductivity of titanium alloys, it is easy to enhance the softening effect due to excessive local temperature rise during processing. Moreover, under high strain rate conditions ($\dot{\varepsilon} = 10\,\mathrm{s}^{-1}$), the flow curve has a certain degree of a jittering phenomenon, and to investigate the reason for this, Fig. 5 shows photographs of the microstructure under different deformation conditions. As shown in Fig. 5a, under the condition of a high strain rate ($\dot{\varepsilon} = 10\,\mathrm{s}^{-1}$), the tissue exhibits local plastic flow. Combining the microstructure of the specimen and the macroscopic morphology in the lower left corner of the picture, it can be clearly seen that there are obvious "bright bands" on the specimen, which may be due to the short deformation time when deforming under large strain rate conditions, a large amount of heat of deformation is not dissipated to make the internal temperature rise of the material too large and eventually lead to local plastic flow inside the material. At low strain rates ($\dot{\varepsilon} \leq 1\,\mathrm{s}^{-1}$), the grains become deformed, the grain boundaries become wider and serrated, and a large number of recrystallized grains appear at the grain boundaries, and the degree of recrystallization increases with decreasing strain rate and decreasing temperature, as shown in Fig. 5b. Zhu et al. [16] found a similar phenomenon during the study of the thermal deformation behavior of Ti40. These typical characteristics of dynamic

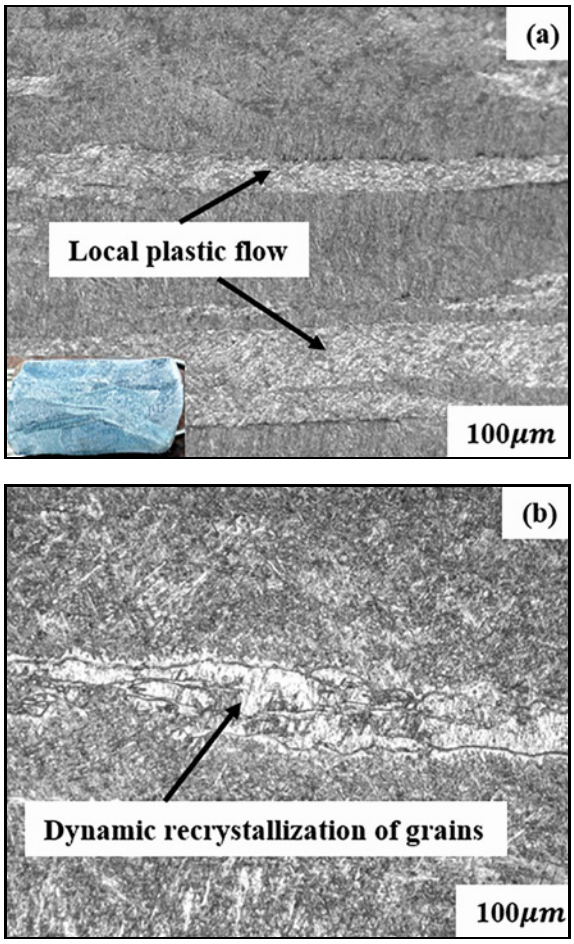

Fig. 5. Microstructure photos of cast TA15 titanium alloy under different deformation conditions: (a)1323 K/10 s^{-1}, and (b) 1423 K/0.1 s^{-1}.

reversion and recrystallization illustrate that at low strain rates, softening of TA15 alloys occurs as a result of dynamic reversion and recrystallization, while at high strain rates, softening of the alloy occurs as a result of local plastic flow due to excessive temperature rise.

3.2. Establishment of the strain-dependent constitutive equation

The material plasticity principal equation represents the relationship between stress and strain during material deformation. In addition, the principal equation can also characterize the relationship between flow stress and deformation parameters, such as deformation temperature and strain rate, which is an effective way to study the material deformation information in depth. The relationship between the flow stress σ, the deformation temperature T, and strain rate $\dot{\varepsilon}$ for the high-temperature case can usually be described by the following equation [17]:

$$\dot{\varepsilon} = AF(\sigma)\exp(-Q/RT), \tag{1}$$

where $F(\sigma)$ is a function of stress. The present equation is a generalized constitutive equation concerning thermoforming. However, the difference in the response characteristics of the thermal parameters due to the difference in materials leads to different forms of the principal equation for different materials. Therefore, the expressions concerning the mathematical relationship between $\dot{\varepsilon}$ and σ are divided into three cases:

(1) In the low-stress region ($\alpha\sigma < 0.8$):

$$\dot{\varepsilon} = A_1\sigma^{n_1}\exp(-Q/RT), \tag{2}$$

(2) In the high-stress region ($\alpha\sigma > 1.2$):

$$\dot{\varepsilon} = A_2\exp(\beta\sigma)\exp(-Q/RT), \tag{3}$$

(3) The entire stress range (hyperbolic sine function equation):

$$\dot{\varepsilon} = A[\sinh(\alpha\sigma)]^n\exp(-Q/RT), \tag{4}$$

where A_1, A_2, A, n_1, n, α, and β are temperature-independent constants, A is the structure factor (s^{-1}), and $a = b/n_1$ is satisfied between a, b, n_1. R is the gas constant (8.314 J mol^{-1} K^{-1}), T is deformation temperature (K), Q is deformation activation energy (J mol^{-1}), and the flow stress σ corresponds to the specified strain condition.

Zener and Hollomon proposed and verified that the relationship between strain rate and temperature can be expressed by a parameter Z [18]:

$$Z = \dot{\varepsilon}\exp\left(\frac{Q}{RT}\right) = A[\sinh(\alpha\sigma)]^n, \tag{5}$$

where the physical meaning of the parameter Z is the temperature-compensated deformation rate factor, and the meanings of the other letters are mentioned above. If the values of the material constants A, Q, n, and α are known, the value of the flow stress σ for the material under arbitrary deformation conditions can be found as follows:

$$\begin{aligned}\sigma &= \frac{1}{\alpha}\left[\sinh^{-1}\left(\frac{Z}{A}\right)^{\frac{1}{n}}\right] \\ &= \frac{1}{\alpha}\left[\sinh^{-1}\left(\frac{\dot{\varepsilon}\exp(Q/RT)}{A}\right)^{\frac{1}{n}}\right].\end{aligned} \tag{6}$$

In order to better reflect the relationship between the flow stress of the material and the thermal processing parameters (strain rate, deformation temperature, and strain), it is important to establish the constitutive equation considering the strain. In this paper, the

Table 3. Stress values of cast TA15 titanium alloy for different deformation conditions at a true strain of 0.5 $\ln\sigma_{0.5}$

T (K)	$\dot{\varepsilon}$ (s^{-1})	$\ln(\dot{\varepsilon})$	$\sigma_{0.5}$ (MPa)	$\ln\sigma_{0.5}$
1323	0.1	−2.303	40.392	3.698632
	1	0	64.226	4.162408
	10	2.303	97.105	4.575793
1373	0.1	−2.303	29.088	3.370326
	1	0	64.987	4.174187
	10	2.303	76.981	4.343559
1423	0.1	−2.303	29.771	3.393535
	1	0	49.991	3.911843
	10	2.303	75.127	4.31918
1473	0.1	−2.303	31.299	3.443586
	1	0	42.133	3.740831
	10	2.303	71.566	4.27062

stress values at a total of 8 strain points from 0.1 to 0.8 (with 0.1 as the interval) are used to calculate the corresponding equation parameters and then establish the principal structure equation considering strain. The specific calculation process is described with strain 0.5 as an example, and the model parameters such as α, n, Q, and A under this strain are obtained by calculation, and so on for other strains.

1. Determine the value of α, taking the natural logarithm for both sides of Eqs. (2) and (3):

$$\ln\dot{\varepsilon} = n_1 \ln\sigma + \ln A_1 - Q/RT, \tag{7}$$

$$\ln\dot{\varepsilon} = \beta\sigma + \ln A_2 - Q/RT. \tag{8}$$

The steady-state stress and strain rates are brought into Eqs. (7) and (8), and the parameter values are obtained in Table 3. The $\ln(\sigma)$–$\ln(\dot{\varepsilon})$ curve and the σ–$\ln(\dot{\varepsilon})$ curve were plotted based on the data in Table 3 and processed as a one-dimensional linear regression using Origin software, as shown in Fig. 6. n_1 and β are the average of the inverse of the slopes of the four lines in Figs. 6a,b, yielding $n_1 = 5.11$, $\beta = 0.09825$, then the value of α is:

$$\alpha = \frac{\beta}{n_1} = 0.0192. \tag{9}$$

2. Determine the values of n and Q. Taking logarithms for both sides of Eq. (4) and assuming that the deformation activation energy is independent on temperature, we obtain:

$$\ln\dot{\varepsilon} = n\ln[\sinh(\alpha\sigma)] + \ln A - Q/RT. \tag{10}$$

The calculated α values, strain rates, and steady-state stresses were brought into Eq. (10) to plot the

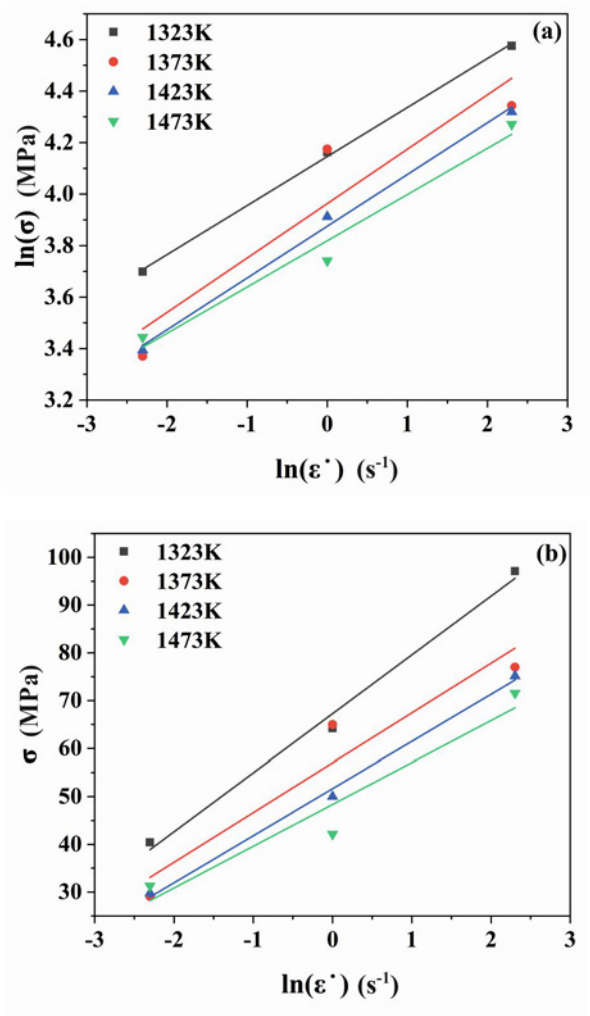

Fig. 6. (a) $\ln(\sigma)$–$\ln(\dot{\varepsilon})$ fitting curve, and (b) σ–$\ln(\dot{\varepsilon})$ fitting curve.

$\ln\dot{\varepsilon}$–$\ln[\sinh(\alpha\sigma)]$ curve and $\frac{1}{T}$–$\ln[\sinh(\alpha\sigma)]$ curve, as shown in Fig. 7. Applying *Origin software* for one-dimensional linear regression processing, the value of the reciprocal of the slope of the line in Fig. 7a is n, and the value of the reciprocal of the slope of each line in Fig. 7b is Q. After calculation, it is obtained that $n = 3.835$ and $Q = 187.760\,\mathrm{kJ\,mol^{-1}}$.

3. Determine the A value: From Eq. (10) and Fig. 7a, the value of $\ln A - Q/RT$ is the intercept of the line in the graph of $\ln\dot{\varepsilon}$–$\ln[\sinh(\alpha\sigma)]$, and the values of R, Q, and T are brought in to find the value of A at different temperatures. After calculation, $A = 5.3 \times 10^6$. Bringing the calculated values of n, A, a, and Q for a strain of 0.5 into Eq. (4), we can find the principal equation for a strain of 0.5 as follows:

$$\dot{\varepsilon} = 5.3 \times 10^6 [\sinh(0.019\sigma)]\, 3.5835 \exp\left(-\frac{187760}{RT}\right). \tag{11}$$

The data under different strain conditions in the

Table 4. Parameter values in the fitting Eq. (12)

	Coefficients						
Material constants	1	ε^1	ε^2	ε^3	ε^4	ε^5	ε^6
α	0.02	–0.04	0.22	–0.67	1.18	–1.09	0.42
n	12.03	–128.19	854.88	–2887.53	5167.34	–4678.77	1690.14
Q	345.08	–434.71	39764.40	–163246.25	333041.61	–330573.28	127579
$\ln A$	27.68	–349.68	3234.81	–13342.95	27289.96	–27133.65	10486.11

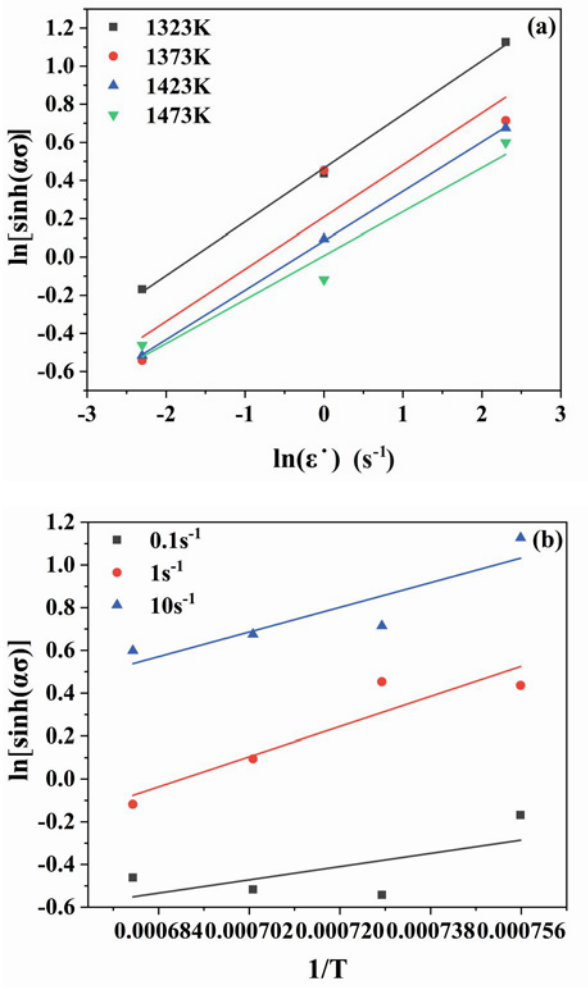

Fig. 7. (a) $\ln\dot{\varepsilon}$–$\ln[\sinh(\alpha\sigma)]$ fitting curve, and (b) $\frac{1}{T}$–$\ln[\sinh(\alpha\sigma)]$ fitting curve.

strain range of 0.1 to 0.8 were processed and calculated by the same method, and the material parameters (n, A, α, and Q), etc., under different strain conditions were obtained as a basis to model each material parameter and to prepare the constitutive equations considering the strain effects. For different material parameters, different sub-polynomials were chosen to construct the parameter models in order to improve their fitting accuracy, and the fitting relationship between the material constants and strains is shown in Fig. 8. The calculated parameter values under different strain conditions are fitted using polynomials with the fitting equation:

$$\begin{aligned}
\alpha &= B_0 + B_1\varepsilon^1 + B_2\varepsilon^2 + B_3\varepsilon^3 + B_4\varepsilon^4 + B_5\varepsilon^5 + B_6\varepsilon^6,\\
n &= C_0 + C_1\varepsilon^1 + C_2\varepsilon^2 + C_3\varepsilon^3 + C_4\varepsilon^4 + C_5\varepsilon^5 + C_6\varepsilon^6,\\
Q &= D_0 + D_1\varepsilon^1 + D_2\varepsilon^2 + D_3\varepsilon^3 + D_4\varepsilon^4 + D_5\varepsilon^5 + D_6\varepsilon^6,\\
\ln A &= E_0 + E_1\varepsilon^1 + E_2\varepsilon^2 + E_3\varepsilon^3 + E_4\varepsilon^4 + E_5\varepsilon^5 + E_6\varepsilon^6.
\end{aligned} \tag{12}$$

The constants in Eq. (12) are shown in Table 4. Finally, the calculated parameter values are brought into Eq. (6), so that the intrinsic equation of TA15 alloy can be established considering the effect of strain. The established constitutive equation considering the effect of strain can accurately describe the rheological behavior of TA15 alloy under the whole stress range.

From Fig. 8a, it can be seen that α shows an increasing trend with increasing strain, and the maximum value is obtained at $\varepsilon = 0.8$ as 0.021. Combining Figs. 8b and 8d, it can be clearly found that the value of activation energy Q shows the same trend as the value of $\ln A$ with strain, and the average value of activation energy Q is 201.957 kJ mol^{-1}. The trend of the n value decreases with increasing strain, and its variation ranges from 5.4 to 3.8, as shown in Fig. 8c.

In summary, the intrinsic equation for the cast TA15 titanium alloy over the entire stress range can be expressed as:

$$\begin{aligned}
\sigma &= \frac{1}{\alpha}\left[\sinh^{-1}\left(\frac{Z}{A}\right)^{\frac{1}{n}}\right],\\
Z &= \dot{\varepsilon}\exp\left(\frac{Q}{RT}\right),\\
\alpha &= B_0 + B_1\varepsilon^1 + B_2\varepsilon^2 + B_3\varepsilon^3 + B_4\varepsilon^4\\
&\quad + B_5\varepsilon^5 + B_6\varepsilon^6,\\
n &= C_0 + C_1\varepsilon^1 + C_2\varepsilon^2 + C_3\varepsilon^3 + C_4\varepsilon^4\\
&\quad + C_5\varepsilon^5 + C_6\varepsilon^6,\\
Q &= D_0 + D_1\varepsilon^1 + D_2\varepsilon^2 + D_3\varepsilon^3 + D_4\varepsilon^4\\
&\quad + D_5\varepsilon^5 + D_6\varepsilon^6,\\
\ln A &= E_0 + E_1\varepsilon^1 + E_2\varepsilon^2 + E_3\varepsilon^3 + E_4\varepsilon^4\\
&\quad + E_5\varepsilon^5 + E_6\varepsilon^6.
\end{aligned} \tag{13}$$

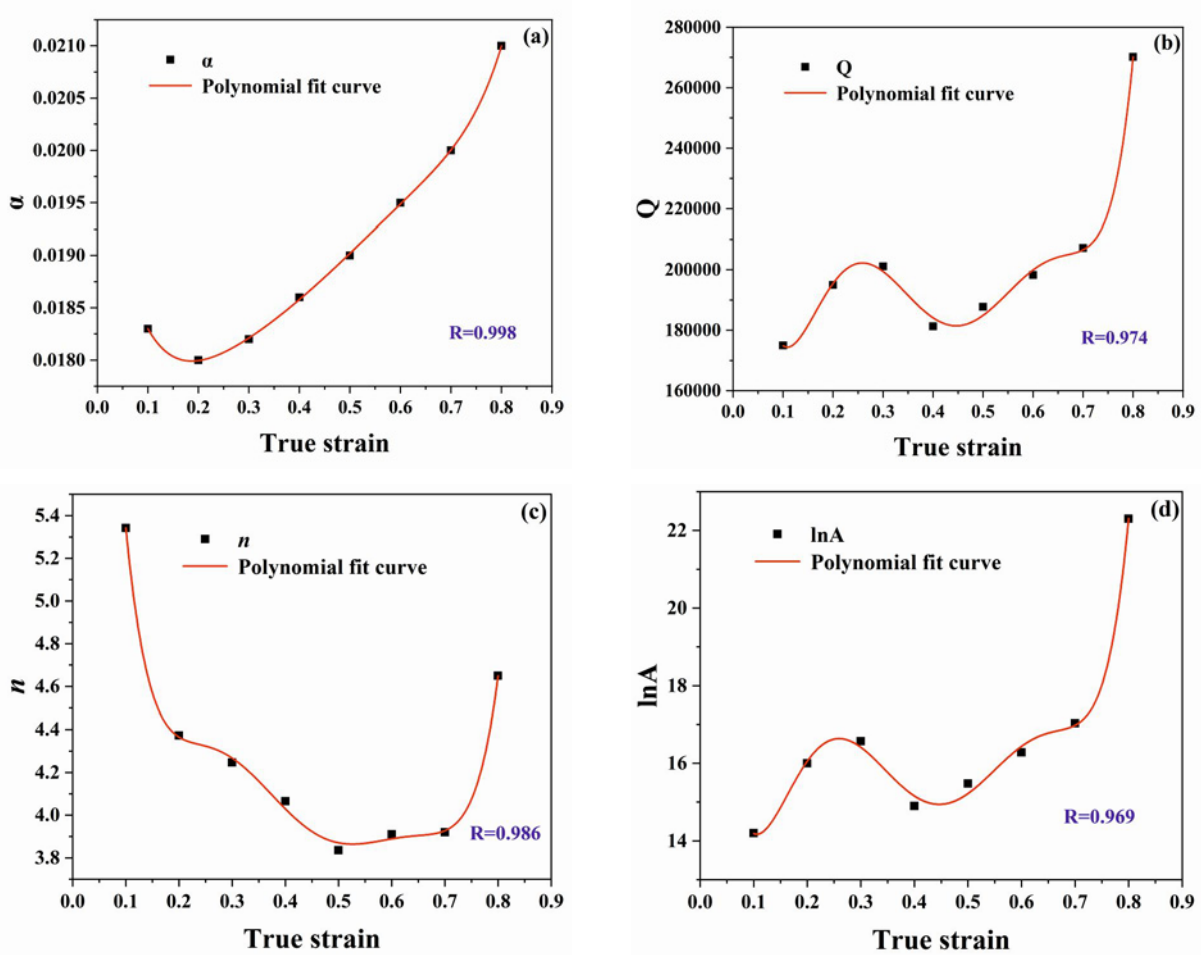

Fig. 8 Relationship between material constants and true strain: (a) α–ε, (b) Q–ε, (c) n–ε, and (d) $\ln A$–ε.

Table 5. Percent error between predicted and measured values of flow stress

Errors (%)	1323 K	1373 K	1423 K	1473 K
0.1	–1.5286	8.9177	1.6004	–4.9923
1.0	–1.5259	–3.3439	0.4955	6.6441
10	–5.7615	8.5631	1.6526	–2.4076

3.3. Prediction accuracy validation of the constitutive equation

To verify the accuracy of the principal structure equations constructed in this study, the measured values of rheological stresses at different deformation temperatures and different strain rates at a true strain of 0.5 were compared with the predicted values, and the errors are shown in Table 5. As can be seen from the table, the error range between the measured and predicted values of flow stress under different deformation conditions is within ± 10 %, which is a small error. The use of correlation coefficient r and average relative error ARE can evaluate the accuracy of the intrinsic structure model more precisely [19]. The average error between the predicted and measured values is calculated according to Eq. (13):

$$\mathrm{ARE} = \frac{1}{M}\sum_{i=1}^{M}\left|\frac{D_i - P_i}{P_i}\right| \times 100, \qquad (14)$$

where M is total number of data, D_i is measured value of flow stress (MPa), and P_i is predicted value of flow stress (MPa).

Combining the data listed in Table 5, the calculation according to Eq. (13) yields ARE = 6.45 %. To better visualize the correlation between the predicted and measured values of flow stress, the measured and predicted values were plotted in horizontal and vertical coordinates (as shown in Fig. 9), and the correlation coefficient was obtained by fitting as $r = 0.95637$.

In summary, the stress values predicted by the as-cast TA15 titanium alloy high-temperature deformation intrinsic constitutive equation constructed in this study have a high correlation with the actual measured values, with small errors and high confidence.

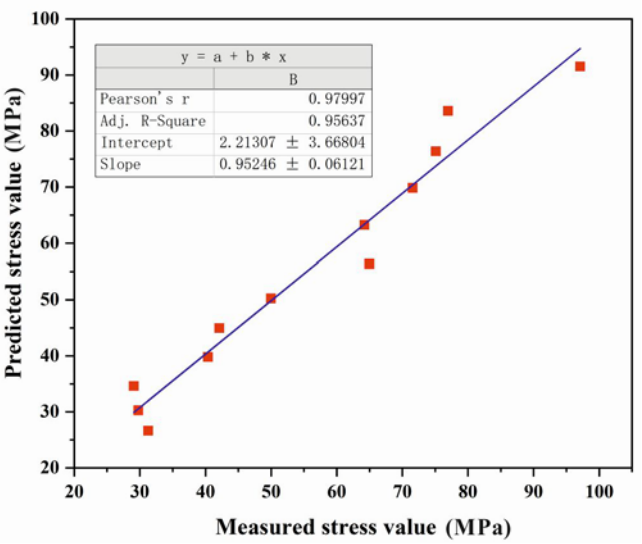

Fig. 9. Correlation between predicted stress values and measured stress values.

3.4. Thermal processing diagram

The use of thermal processing diagrams to study materials can be more intuitive to observe the microscopic deformation mechanism in the processing stability region and the non-safety region such as plastic destabilization and cracking, which can help processors to optimize the processing process of materials and obtain more ideal material organization and properties. The thermal processing diagram is a superposition of the power dissipation diagram and the instability diagram, where the power dissipation diagram reveals the tissue evolution of the material, and the instability diagram describes the "safe zone" and "non-safe zone" during the plastic deformation of the material; combined with the microstructure observation, it can characterize the tissue evolution of the material during the high-temperature deformation process with respect to the influence of processing parameters.

3.4.1. Energy dissipation diagram

Prasad et al. [20] established a dynamic material model (DMM) based on the theory of irreversible thermodynamics and physical system simulations, etc., from which it is known that the energy dissipation P in the process of thermal processing of materials is mainly divided into two parts, namely, the energy consumed during plastic deformation G and the energy consumed during tissue transformation J [21] so that the dissipated energy P can be expressed as:

$$P = \sigma\dot{\varepsilon} = G + J = \int_0^{\dot{\varepsilon}} \sigma \mathrm{d}\varepsilon + \int_0^{\sigma} \dot{\varepsilon} \mathrm{d}\sigma, \tag{15}$$

where G is the dissipation (energy dissipated during plastic deformation), J is the dissipation coefficients (energy dissipated during microstructure evolution during deformation), σ is the rheological stress, and $\dot{\varepsilon}$ is the strain rate.

The strain rate sensitivity exponent m determines the distribution of these two energies [22]:

$$m = \frac{\partial J}{\partial G} = \frac{\dot{\varepsilon}\partial\sigma}{\sigma\partial\dot{\varepsilon}} = \frac{\partial \ln\sigma}{\partial \ln\dot{\varepsilon}}. \tag{16}$$

For a given temperature T and strain ε, J can be expressed as:

$$J = \int_0^{\sigma} \dot{\varepsilon} \mathrm{d}\sigma = \frac{m\sigma\dot{\varepsilon}}{m+1}. \tag{17}$$

When m is equal to 1, the material exhibits an ideal linear dissipative state and the dissipative coefficients J reach a maximum value of $J_{\max}$:

$$J_{\max} = \frac{\sigma\dot{\varepsilon}}{2}. \tag{18}$$

Therefore, the energy dissipation rate η can be expressed as:

$$\eta = \frac{J}{J_{\max}} = \frac{2m}{m+1}, \tag{19}$$

where m is the strain rate sensitivity exponent.

For steady-state rheological stresses, the value of the strain rate sensitivity exponent ranges from 0 to 1. When $m = 0$, it means that the system does not dissipate energy; when $m = 1$, it indicates that the material tends to a viscous fluid state. The parameter η represents the different deformation mechanisms reflected by the workpiece for a given different deformation temperature and strain rate, as well as the evolutionary state of the workpiece's own organization. The equivalence curve between temperature and strain rate and dissipation rate under a given strain is the power dissipation diagram, which plays a key role in the selection of optimal thermal deformation parameters during thermal processing.

Figure 10 shows the energy dissipation diagrams of the cast TA15 titanium alloy during thermal deformation when the true strain is 0.1, 0.3, 0.5, and 0.8. As can be seen in Fig. 10, the peak of the energy dissipation rate when the material is deformed plastically under different deformation conditions occurs at low temperatures and low strain rates. This is mainly due to the fact that when the strain rate is low, the material has sufficient deformation time to undergo plastic deformation.

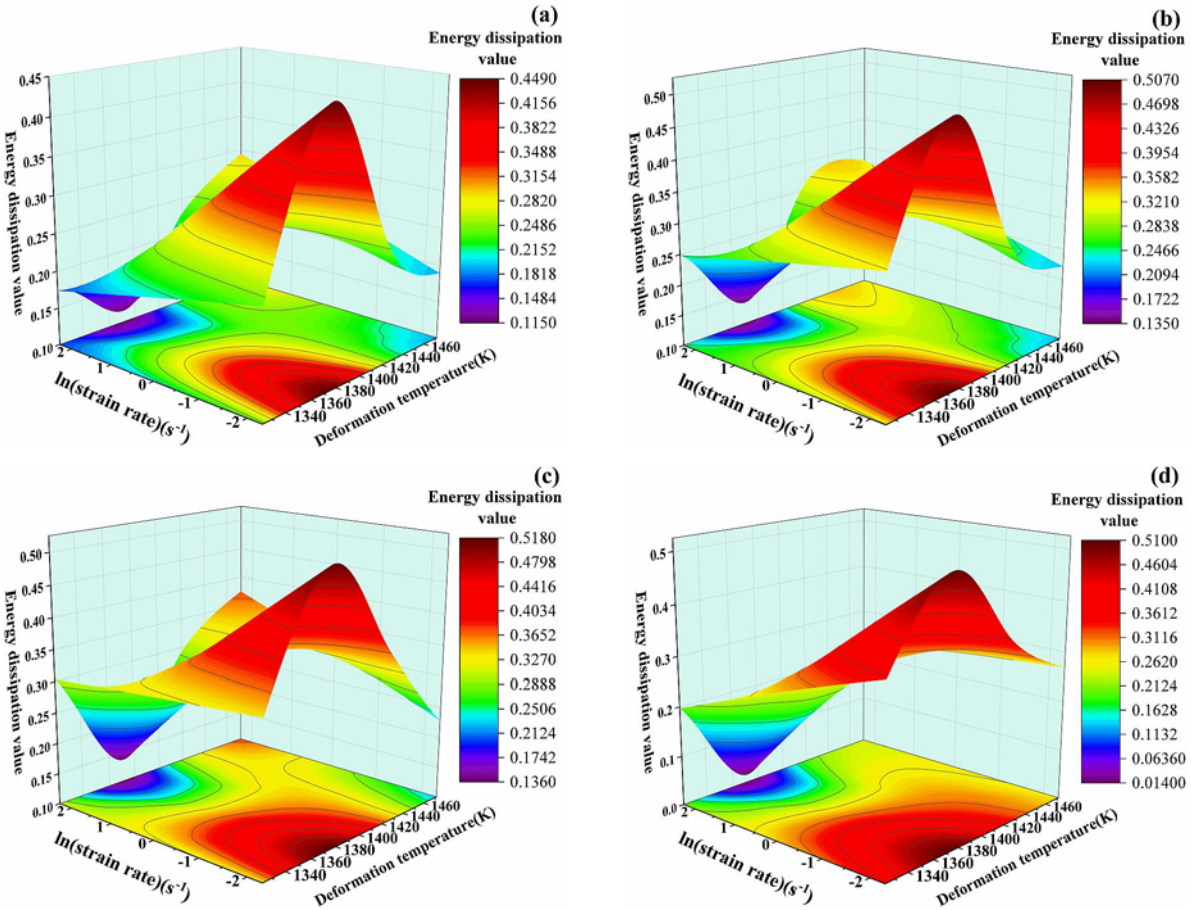

Fig. 10. Energy dissipation at different strains during thermal deformation of cast TA15 titanium alloy:(a) 0.1, (b) 0.3, (c) 0.5, and (d) 0.8.

3.4.2. Plastic instability diagram

The processability of a material cannot be determined by the power dissipation rate alone, but also needs to be combined with the organization of the material in high temperature plastic deformation. The plastic instability diagram is a parameter that judges the likelihood of material instability during processing and deformation. The instability diagram can be used to infer the instability and safety regions under different machining parameters, providing a basis for optimization of the machining process. Prasad proposed a destabilization criterion [23]:

$$\xi(\dot{\varepsilon}) = \frac{\partial\left(\ln\dfrac{m}{m+1}\right)}{\partial \ln \dot{\varepsilon}} + m < 0, \qquad (20)$$

where $\xi(\dot{\varepsilon})$ is a temperature-dependent function of strain rate.

A negative value of $\xi(\dot{\varepsilon})$ indicates the occurrence of rheological instability during the deformation process, while the determination of the form of instability is determined analytically based on the specific tissue results. The processing instability diagram is obtained by plotting the contours of the instability parameters with respect to the strain rate $\dot{\varepsilon}$ and the temperature T. As shown in Fig. 11, the plastic instability diagrams of the cast TA15 titanium alloy during hot deformation when the true strain is 0.1, 0.3, 0.5, and 0.8. It can be seen from the figure that the minimum value of the instability criterion appears at high strain rate conditions. This is mainly due to the short deformation time of TA15 titanium alloy when the strain rate is high, and the poor heat dissipation of this material makes the heat of deformation unable to be dissipated, resulting in local plastic flow within the material and plastic destabilization of the material.

The corresponding thermal processing diagrams are obtained by superimposing the energy dissipation diagrams of each strain and the two-dimensional contour diagrams of the plastic instability diagrams. The thermal processing diagrams at strain 0.3 and strain 0.5 are shown in Fig. 12. The contour values are the same power dissipation coefficients, and the "cool color" region represents the instability region.

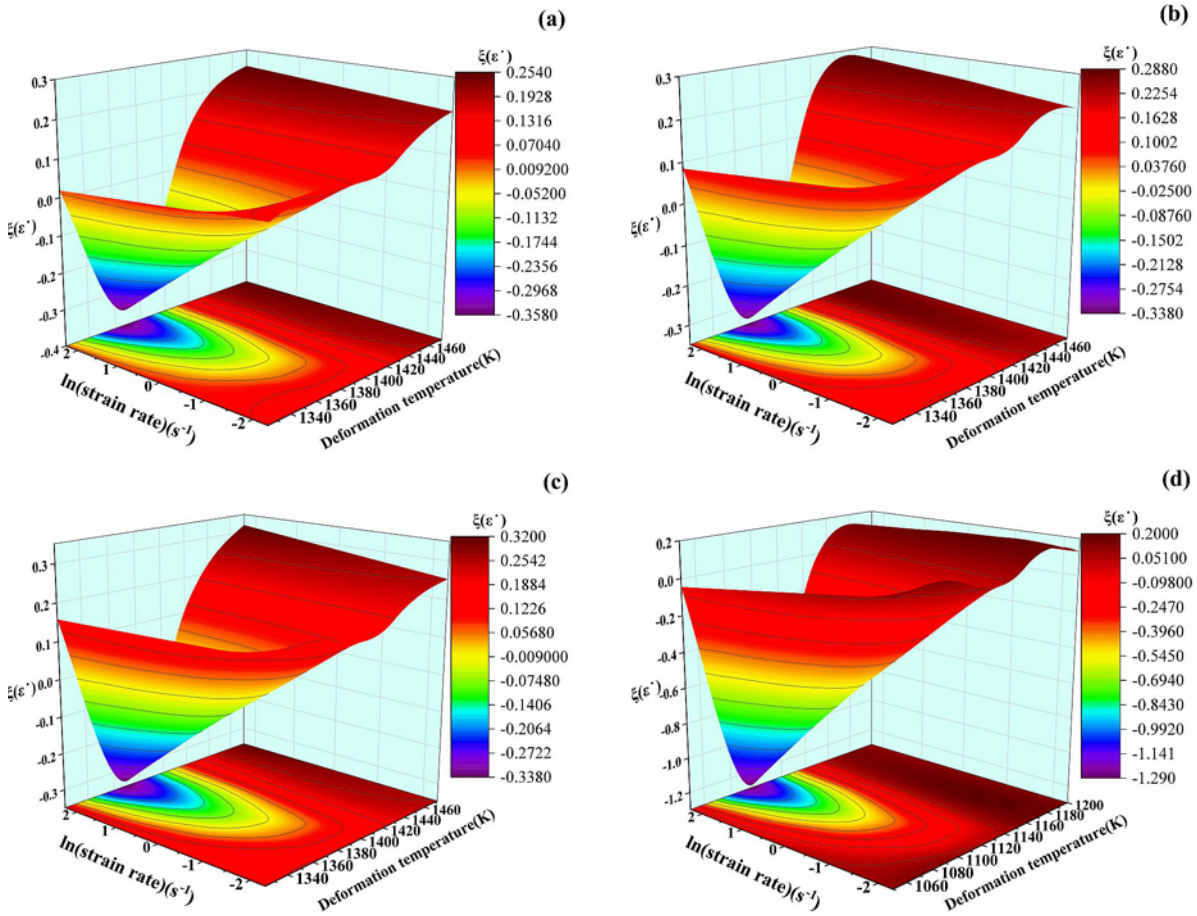

Fig. 11. Plastic destabilization diagram of cast TA15 titanium alloy at different strains during thermal deformation: (a) 0.1, (b) 0.3, (c) 0.5, and (d) 0.8.

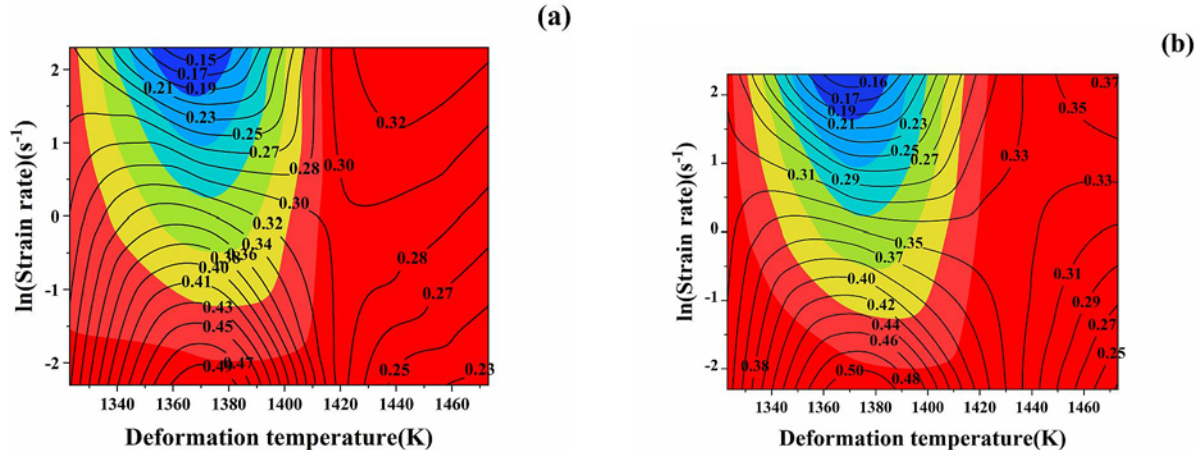

Fig. 12. Thermal processing diagram of cast TA15 titanium alloy under different strains during thermal deformation: (a) 0.3 and (b) 0.5.

3.4.3. Analysis of thermal processing diagrams

In this study, the data of true strain 0.3 and 0.5 were selected to establish the thermal processing diagram, and the thermal processing diagram of TA15 titanium alloy deformed in the range of temperature 1323–1473 K and strain rate 0.1–10 s^{-1} was plotted, as shown in Fig. 12. As can be seen in Fig. 12, the degree of power dissipation increases with the strain rate; as the strain increases, the power dissipation also increases. At a strain of 0.5, a peak power dissipation

region of 0.50 can be observed from the thermal processing diagram, occurring at a deformation condition of 1373 K/0.1 s^{-1}. In addition, under the low temperature and high strain rate conditions, the processing map shows the instability zone, and the area of the instability zone increases with the strain. Therefore, during processing, machining production under the conditions of thermal processing parameters contained in the destabilization region should be avoided. In order to further determine the deformation mechanism of TA15 titanium alloy in these regions and also to determine the processing parameters in the optimized regions of the thermal processing diagram, the microstructure of the safe and destabilized regions in the thermal processing diagram will be analyzed.

From Fig. 12, it can be seen that the safety zone of material deformation of cast TA15 titanium alloy at strain conditions of 0.3 and 0.5 is in a region that can be divided into two regions, one region is in the range of temperature conditions 1333–1043 K and strain rate 0.1–0.8 s^{-1}; the other region is in the range of temperature conditions 1403–1473 K and strain rate 0.1–10 s^{-1}. The power dissipation rate is approximately between 0.2 and 0.5. The peak regions of power dissipation appear at low strain rate conditions. This all indicates that the alloy has better processing properties in these regions.

In order to reveal the mechanism of tissue deformation in the region where the peak power dissipation rate occurs in the as-cast TA15 titanium alloy, its microstructure was observed and analyzed, as shown in Fig. 13. As seen in Fig. 13a, the grain boundaries are deformed and show jaggedness, and there are a small number of smaller sized recrystallized grains at the grain boundaries, which is typical of dynamic recrystallization. In combination with the effect of dynamic reversion, it contributes to the high energy dissipation rate in the thermal processing diagram under this deformation condition. In Fig. 13b, it can be seen that the size of the recrystallized grains increases significantly, and the shape is irregular. This is due to the larger recrystallization driving force obtained at higher temperatures, which drives the growth of recrystallized grains. From the above microstructure observation and analysis, it can be concluded that the alloy is prone to dynamic recrystallization when the strain rate is higher, which is also related to the fact that the low strain rate provides more deformation time and substructure. Generally speaking, the appearance of dynamic recrystallized grains can refine the organization and promote the microstructure of the material, which is beneficial to the thermal deformation process of the alloy, so as to finally obtain a good performance of the alloy material, therefore, the appropriate increase in deformation temperature under low strain rate conditions can effectively improve the properties of the alloy organization, and the hot

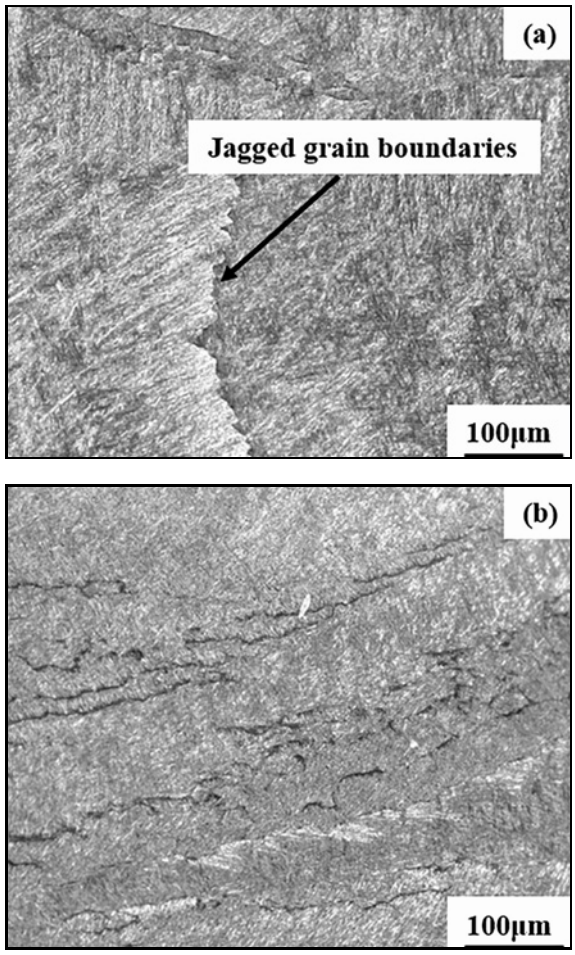

Fig. 13. Microstructure of specimens at 1323 K/0.1 s^{-1} and 1473 K/0.1 s^{-1} for deformation conditions.

processing diagram also effectively confirms this conclusion.

As can be seen in the thermal processing diagram shown in Fig. 12, the destabilization zone is located approximately in the shaded region of temperature conditions 1343 to 1393 K and strain rate conditions 1.0 to 10 s^{-1}. In order to reveal the deformation mechanism of the destabilized region, Fig. 14 shows a tissue photograph of the destabilized region that is in the thermal processing diagram. Figure 14a shows the organization of the alloy under deformation conditions at 1323 K/10 s^{-1}. The banded area formed by local plastic flow can be clearly seen in the picture, which may be related to the poor thermal conductivity of the titanium alloy and the local temperature rise at high strain rates. However, in Fig. 14b, the presence of deformation instability was observed in the microstructure of the alloy and cracking was found on the surface of the alloy. Local plastic flow and cracking phenomena can reduce the performance of the material or even lead to failure, and these destabilization phenomena should be given to avoid.

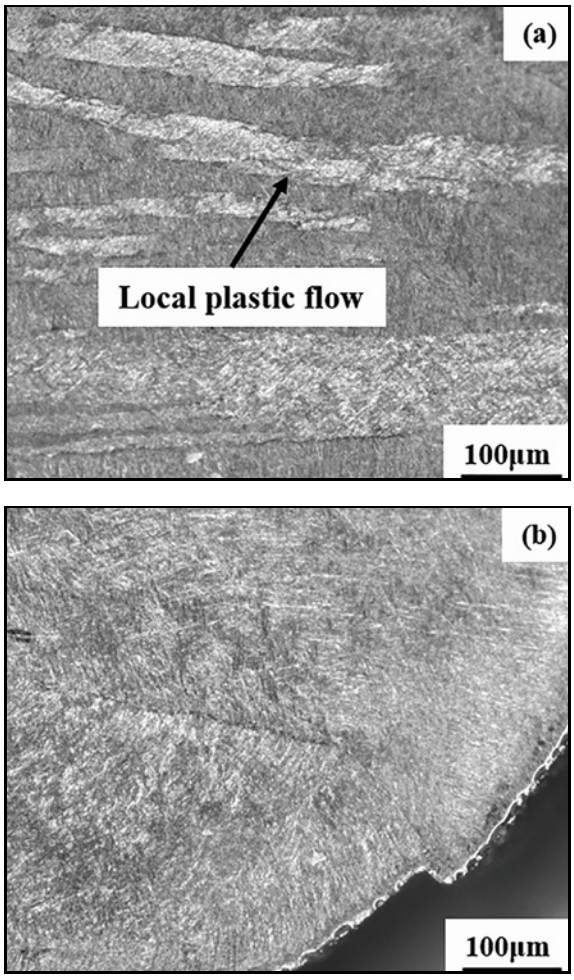

Fig. 14. Local plastic flow at deformation conditions of 1323 K/10 s^{-1} and deformation instability and cracking at deformation conditions of 1373 K/10 s^{-1}.

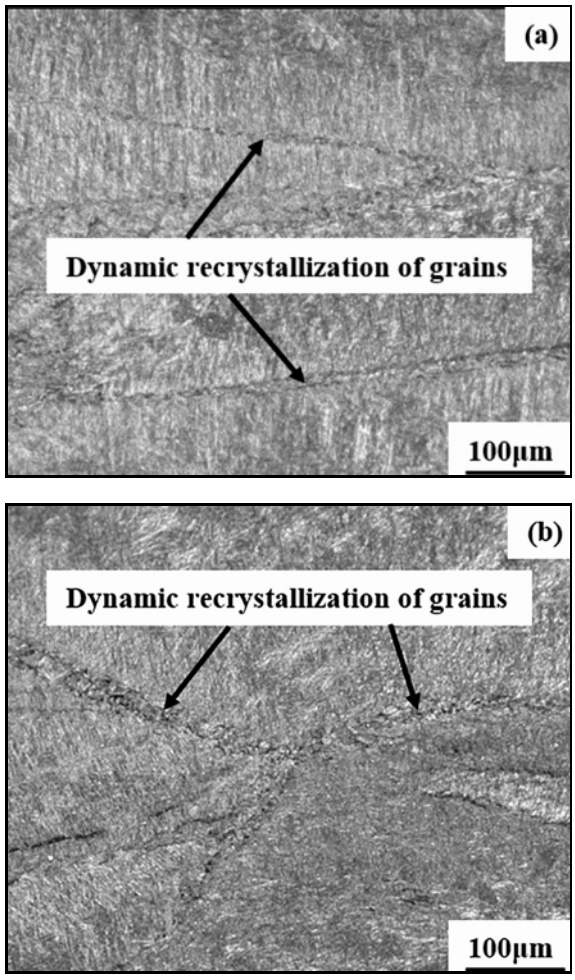

Fig. 15. Microstructure of cast TA15 titanium alloy after deformation within a reasonable processing range: (a) 1373 K/1 s^{-1} and (b)1423 K/0.1 s^{-1}.

Based on the above microstructure observation and analysis, the thermal deformation parameters of cast TA15 titanium alloy have a great influence on the thermal deformation behavior, and the suitable thermal deformation parameter conditions for TA15 alloy are derived, with deformation temperature of 1373–1423 K, strain rate of 0.1–1.0 s^{-1}, and strain of 0.92. This is because the alloy in the temperature range of 1323–1393 K, the strain rate range of 1–10 s^{-1} deformation conditions for the destabilization zone; and when the temperature range is greater than 1423 K or even up to 1473 K, although in the processing chart safety zone, but the temperature is too high so that the grain growth, organization coarsening, is also not conducive to the improvement of material properties. At smaller deformation amounts, only a small amount of recrystallized grains of TA15 alloy exist, and the degree of dynamic recrystallization is insufficient, which has limited improvement of material properties; at the same time, too much deformation can lead to tissue cracking and material failure. Figure 15 shows a photo of the material organization under suitable deformation conditions, from which it can be clearly seen that the organization is uniformly deformed, with a large number of fine recrystallized grains at grain boundaries, especially at trigonal grain boundaries and a sufficient degree of dynamic recrystallization; from the macroscopic aspect, there is also no presence of instability phenomena such as cracking on the material surface, and the deformation is good. Therefore, TA15 alloy is considered to be a more suitable thermal processing parameter at a temperature of 1373–1423 K and a strain rate of 0.1–1.0 s^{-1}.

4. Conclusions

In this study, the cast TA15 titanium alloy was taken as the research object, and the high temperature deformation behavior of the alloy was studied based

on the hot compression simulation experiment. According to the constitutive equation, thermal processing map, and microstructure, the following conclusions were drawn:

(1) The flow stress of cast TA15 titanium alloy decreases with the decrease of strain rate and the increase of deformation temperature, showing different degrees of softening. Through the observation and analysis of the tissues, the softening effect occurs in TA15 alloy at low strain rate conditions due to dynamic reversion and recrystallization, while at high strain rate conditions, the softening occurs in TA15 alloy due to local plastic flow caused by excessive temperature rise.

(2) Based on the thermal simulation compression experimental data, the intrinsic constitutive equation of the cast TA15 titanium alloy was established by combining the effect of strain on the intrinsic constitutive relationship model. The error analysis of the model was also carried out, and the correlation coefficient r was 0.95637, and the average relative error ARE was 6.45 %. It can be seen that this instantonal equation can accurately describe the rheological behavior of cast TA15 titanium alloy under the whole stress range. The constitutive equation (Eq. (13)) is:

$$\begin{aligned}
\sigma &= \frac{1}{\alpha}\left[\sinh^{-1}\left(\frac{Z}{A}\right)^{\frac{1}{n}}\right],\\
Z &= \dot{\varepsilon}\exp\left(\frac{Q}{RT}\right),\\
\alpha &= B_0 + B_1\varepsilon^1 + B_2\varepsilon^2 + B_3\varepsilon^3 + B_4\varepsilon^4\\
&\quad + B_5\varepsilon^5 + B_6\varepsilon^6,\\
n &= C_0 + C_1\varepsilon^1 + C_2\varepsilon^2 + C_3\varepsilon^3 + C_4\varepsilon^4\\
&\quad + C_5\varepsilon^5 + C_6\varepsilon^6,\\
Q &= D_0 + D_1\varepsilon^1 + D_2\varepsilon^2 + D_3\varepsilon^3 + D_4\varepsilon^4\\
&\quad + D_5\varepsilon^5 + D_6\varepsilon^6.\\
\ln A &= E_0 + E_1\varepsilon^1 + E_2\varepsilon^2 + E_3\varepsilon^3 + E_4\varepsilon^4\\
&\quad + E_5\varepsilon^5 + E_6\varepsilon^6.
\end{aligned} \tag{13}$$

(3) Combining the hot compression test data and the dynamic material model, the thermal processing diagram of the cast TA15 titanium alloy was constructed. When the deformation temperature is at 1323–1393 K and the strain rate is 1.0–10 s^{-1}, the alloy is in the instability region; the area of the instability region increases with the strain, and the instability mechanism is mainly local plastic flow and surface cracking. The peak power dissipation in the safety zone occurs within the thermal processing diagram at strain with a value of 0.50. The high dissipation rate is related to the dynamic recrystallization of the material, and the degree of recrystallization increases with the deformation temperature.

(4) The ideal processing window for cast TA15 titanium alloy is: deformation temperature 1373–1423 K, strain rate 0.1–1.0 s^{-1}.

Acknowledgements

The authors thank the Applied Basic Research Program of Shanxi Province (No. 202203021211208 and 20210302123203), and the National Natural Science Foundation of China (No. 51501122 and U1910213) for financial support.

References

[1] Y. Wang, J. C. Zhu, Z. H. Lai, X. Cao, Hot compressive deformation behaviour and microstructural variation of TA15 titanium alloy, Met. Sci. J. 21 (2005) 1466–1470. https://doi.org/10.1179/174328405X71756

[2] Z. C. Sun, S. S. Guo, H. Yang, Nucleation and growth mechanism of α-lamellae of Ti alloy TA15 cooling from an $\alpha+\beta$ phase field, Acta Mater. 61 (2013) 2057–2064. https://doi.org/10.1016/j.actamat.2012.12.025

[3] X. L. Xu, Q. Y. Liu, J. Wang, X. P. Ren, H. L. Hou, The heat treatment improving the mechanical and fatigue property of TA15 alloy joint by friction stir welding, Mater. Charact. 180 (2021) 111399. https://doi.org/10.1016/j.matchar.2021.111399

[4] Y. X. Li, P. F. Gao, J. Y. Yu, S. Jin, S. Q. Chen, M. Zhan, Mesoscale deformation mechanisms in relation with slip and grain boundary sliding in TA15 titanium alloy during tensile deformation, J. Mater. Sci. Technol. 98 (2022) 72–86. https://doi.org/10.1016/j.jmst.2021.05.008

[5] P. F. Gao, G. Qin, X. X. Wang, Y. X. Li, J. S. Li, Dependence of mechanical properties on the microstructural parameters of TA15 titanium alloy with tri-modal microstructure, Mater. Sci. Eng. A 739 (2018) 203–213. https://doi.org/10.1016/j.msea.2018.10.030

[6] Q. Ma, K. Wei, Y. Xu, L. J. Zhao, X. Zhang, Exploration of the static softening behavior and dislocation density evolution of TA15 titanium alloy during double-pass hot compression deformation, J. Mater. Res. Technol. 18 (2022) 872–881. https://doi.org/10.1016/j.jmrt.2022.02.122

[7] K. H. Wang, G. Liu, K. Huang, Denis J. Politis, L. L. Wang, Effect of recrystallization on hot deformation mechanism of TA15 titanium alloy under uniaxial tension and biaxial gas bulging conditions, Mater. Sci. Eng. A 708 (2017) 149–158. https://doi.org/10.1016/j.msea.2017.09.128

[8] T. Yasmeen, Z. T. Shao, L. Zhao, P. Gao, J. G. Lin, J. Jiang, Constitutive modelling for the simulation of the superplastic forming of TA15 titanium alloy, Int. J. Mech. Sci. 164 (2019) 105178. https://doi.org/10.1016/j.ijmecsci.2019.105178

[9] A. Arab, P. W. Chen, Y. S. Guo, Effects of microstructure on the dynamic properties of TA15 titanium alloy, Mech. Mater. 137 (2019) 103121.1–103121.10. https://doi.org/10.1016/j.mechmat.2019.103121

[10] Y. C. Zhu, J. X. Fan, Z. L. Li, Y. Y. Luo, Y. Niu, Study of strain rate sensitivity exponent and strain hardening exponent of typical titanium alloys, Mater. Today Commun. 30 (2022) 103060. https://doi.org/10.1016/j.mtcomm.2021.103060
[11] T. X. Wang, S. Q. Lu, K. L. Wang, D. L. Ouyang, Q. Yao, Hot deformation behavior and processing parameter optimization of Ti60 alloy, Rare Met. Mater. Eng. 49 (2020) 3552–3561. (in Chinese)
[12] P. P. Yao, Research on high temperature deformation mechanism and heat treatment process of TA15 titanium alloy, Hefei Univ. Technol., 2015. (in Chinese)
[13] G. Z. Quan, Y. Wang, J. Zhou, Y. S. Xiong, Response rule of strain rate sensitivity of TA15 to deformation temperature, strain and strain rate, Mater. Heat Treat. 40 (2011) 48–49+53. https://doi.org/10.14158/j.cnki.1001-3814.2011.20.028
[14] A. A. Khamei, K. Dehghani, Modeling the hot-deformation behavior of $Ni_{60wt\%}$ –$Ti_{40wt\%}$ intermetallic alloy, J. Alloys Compd. 490 (2010) 377–381. https://doi.org/10.1016/j.jallcom.2009.09.187
[15] W. P. Wang, M. Wan, X. D. Wu, K. S. Diao, Experimental study of strain rate sensitivity of automotive steel sheet, J. Plast. Eng. 19 (2012) 84–89. (in Chinese) https://doi.org/10.3969/j.issn.1007-2012.2012.06.017
[16] Y. C. Zhu, W. D. Zeng, Y. Q. Zhao, Y. Shu, X. M. Zhang, Effect of processing parameters on hot deformation behavior and microstructural evolution during hot compression of Ti40 titanium alloy, Mater. Sci. Eng. A 552 (2012) 384–391. https://doi.org/10.1016/j.msea.2012.05.055
[17] Z. J. Gronostajski, Development of constitutive equations of copper-silicon alloys, J. Mater. Process. Technol. 60 (1996) 621–627. https://doi.org/10.1016/0924-0136(96)02396-5
[18] X. M. Zhang, F. Y. Cao, H. Y. Yue, Y. C. Feng, E. J. Guo, F. W. Kang, Establishment of constitutive equations of TC11 alloy during hot deformation, Rare Met. Mater. Eng. 42 (2013) 937–941. (in Chinese)
[19] J. N. Mei, F. Xue, T. D. Wu, N. Wei, Z. Cai, Establishment of constitutive equations of FeCrNiMn high entropy alloy, Mater. Rep. 35 (2021) 336–341. (in Chinese)
[20] Y. V. R. K. Prasad, H. L. Gegel, S. M. Doraivelu, J. C. Malas, J. T. Morgan, K. A. Lark, D. R. Barker, Modeling of dynamic material behavior in hot deformation: Forging of Ti-6242, Metall. Trans. A 15 (1984) 1883–1892. https://doi.org/10.1007/BF02664902
[21] Y. N. Zhao, S. Y. Jiang, Y. Q. Zhang, X. M. Zhu, Hot deformation behavior and processing map of NiTi shape memory alloy, Appl. Sci. Technol. 44 (2017) 76–81. (in Chinese)
[22] J. H. Peng, Q. J. Sun, J. W. Zhou, C. Wen, H. Xu, X. Ma, High temperature thermal deformation and processing of TC4-DT titanium alloy, Trans. Nonferrous Met. Soc. China 32 (2022) 994–1003. (in Chinese) https://doi.org/10.11817/j.ysxb.1004.0609.2021-37909
[23] Y. V. R. K. Prasad, K. P. Rao, S. Sasidhara, Hot Working Guide: Compendium of Processing Maps, 2nd ed., ASM International, 2015.